# Catalysis Science & Technology

Accepted Manuscript






ROYAL SOCIETY OF CHEMISTRY

www.rsc.org/catalysis

Journal Name

RSCPublishing

ARTICLE

# Discrimination of mechanism of $CH_4$ formation in Fischer-Tropsch synthesis on Co catalysts: A combined approach of DFT, kinetic isotope effects and kinetic analysis

Cite this: DOI: 10.1039/x0xx00000x

Received 00th January 2012,
Accepted 00th January 2012

DOI: 10.1039/x0xx00000x

www.rsc.org/

Yanying Qi[a], Jia Yang[a,b], Xuezhi Duan[a,c], Yi-An Zhu[c], De Chen[a]*, Anders Holmen[a]*

The mechanism of $CH_4$ formation during Fischer-Tropsch synthesis on cobalt has been studied. DFT, kinetic isotope effect and kinetic analysis are combined to discriminate between possible reaction routes of $CH_4$ formation on Co catalysts. Nine direct reaction mechanisms were proposed from 21 elementary steps. They were first screened by DFT calculations in which the activation energies as well as free energy profiles in each direct mechanism were compared, resulting in a reduction to six reaction mechanisms. Additional reduction was based on the kinetic analysis where the reaction order was used as a descriptor. Subsequently, the kinetic isotope effect (KIE) values were calculated and compared to our previous SSITKA results. Finally, the dominating reaction route was suggested, which follows the initial elementary steps with H-assisted CO activation to form HCOH via HCO as an intermediate. It then proceeds through HCOH dissociation into CH followed by stepwise hydrogenation to $CH_4$.

## 1. Introduction

The Fischer-Tropsch (F-T) process converts synthesis gas into hydrocarbons and oxygenates. It provides an alternative route for production of liquid fuels from coal, natural gas and biomass.[1-3]. The commonly used F-T catalysts are iron and cobalt, depending on the $H_2$ to CO ratio of the syngas used. Cobalt is considered to be the most favourable metal for synthesis of long-chain hydrocarbons from natural gas-based synthesis gas because of its high catalytic activity, high selectivity to linear paraffins, high resistance towards deactivation and low water-gas shift activity[4-8]. The carbon number distribution of Fischer-Tropsch products is usually described by a simple statistical model, the Anderson-Schulz-Flory (ASF) distribution. A usual deviation from the ASF distribution is a relatively high selectivity of methane which is an unwanted byproduct in the process[9]. Therefore, a better understanding of the mechanism of methane formation on Co catalysts is desired, aiming for optimization and design of FT catalysts.

In the recent decade, DFT calculations have increasingly been employed to investigate the mechanism of methane formation on Co catalysts. For example, Hu et al. reported that $CH_3$ hydrogenation is the most difficult step during the stepwise hydrogenation into $CH_4$. The effective barrier for $CH_4$ formation is a good descriptor for the methane production rate, and it suggests that an increase of the binding strength of C+4H will suppress the $CH_4$ selectivity[10-11]. Li et al. pointed out that the structure sensitivity of the CO methanation is ascribed to that of CO dissociation, in which both the direct CO dissociation and the H-assisted dissociation through the HCO intermediate were considered[12]. In fact, CO dissociation proceeds by different reaction pathways, such as direct CO dissociation and H-assisted dissociation through HCO or COH intermediates which may be further hydrogenated, leading to the evolution of several intermediates (e.g., HCO, COH, HCOH, $CH_2O$ and $CH_2OH$). However, a systematic investigation of all possible reaction routes for methane formation involving such $CH_xO$ intermediates is still missing.

The mechanism for methane formation during F-T synthesis on Co catalysts is complicated, involving different CO activation pathways, reaction routes for $CH_x$ formation from $CH_xO$ and sequential $CH_x$ hydrogenation steps. For the CO activation mechanism, the dissociation of the C-O bond may occur through either the direct CO dissociation mechanism or the H-assisted dissociation mechanism[13-18]. It represents a great challenge for discrimination of possible reaction routes for such complex reaction systems, and it seems not possible to use one single method to discriminate between possible mechanisms. Interestingly, combining DFT calculations with experimental studies are a prevalent way to discriminate between reaction mechanisms[14, 19, 20]. The steady-state isotopic transient kinetic analysis (SSITKA) is a powerful experimental tool to distinguish between the contribution of intrinsic activity and the coverage of intermediates[4, 5, 21-22]. In our recent work[23], DFT calculations, SSITKA experiments and kinetic analysis were combined to study the CO activation mechanism. The results showed that H-assisted CO dissociation by HCO intermediate is

a dominating CO activation pathway, and two carbon pools, namely $CH_2O$ and $CH_x$, could be related to methane formation. In order to obtain the detailed mechanism of methane formation, the elementary reaction steps including the stepwise hydrogenation of HCO, COH and $CH_x$ as well as the dissociation of HCO and COH will be further studied by using the above combined approach.

Moreover, both hexagonal close-packed (hcp) and face-centred cubic (fcc) Co catalysts are simultaneously observed during F-T synthesis. It has been claimed that the hcp Co catalysts show higher FTS activity[24-29]. The intrinsic activity increases with increasing Co particle size for particles smaller than 6-7nm possibly because the smaller particles have strongly bonded carbon and oxygen surface species acting as site blocking species, and is more easily oxidized by water vapour [30, 4, 5, 31]. The large-sized cobalt particles mainly expose flat surface (such as Co(0001) facets). For the above reasons, employing the large-sized Co catalysts for SSITKA experiments and modelling the Co(0001) surface for CO activation mechanism by DFT calculations, were performed in our previous work[23].

The present work deals with a combined approach of DFT, kinetic isotope effects and kinetic analysis to further discriminate the mechanism of methane formation. Nine possible direct reaction mechanisms for methane formation were proposed by analysing the possible reaction routes of the intermediates. The activation energies of the elementary steps were first calculated by DFT calculations and then compared in order to exclude some reaction mechanisms. Subsequently, the Langmuir-Hinshelwood (L-H) rate expressions based on CO conversion for the other direct reaction mechanisms were derived, and a comparison between the rate expressions and experimental observations reduced the possible reaction mechanisms even further. The kinetic isotope effects (KIE) of the three possible reaction mechanisms were estimated by DFT calculations. The results were compared with experimental KIEs and the results of our previous SSITKA experiments. The dominating methane formation pathway and the kinetically relevant steps in the reaction mechanism were suggested by a combined DFT calculations, kinetic analysis and kinetic isotope effect.

## 2. Model and Methods

All the spin-polarized DFT calculations were performed in the Vienna Ab Initio Simulation Package (VASP)[32-35]. The Brillouin zone was sampled by 5×5×1 k-point, which was proved to be efficient for the cell[36]. PBE[37] functional was utilized with the first order Methfessel-Paxton method for the electron smearing. The interactions between ion cores and valence electrons were described by the projector augmented wave (PAW) method [38], with a plane wave energy cutoff of 450 eV. Calculations were converged until all forces on the atoms were lower than 0.01 eV/Å. Convergence tests of the calculation parameters were performed and also confirmed by the literature[4, 12, 39]. Co(0001) surface was modeled by p (2×2) unit cell of eight layers and approximately 10 Å of vacuum spacing between the successive metal slabs. With this unit cell, adsorption energies were converged within 0.06 eV with respect to the p(3×3) unit cell. The top four layers were allowed to relax, while the bottom layers were fixed to their crystal positions with the calculated lattice parameter (2.49 Å), which is very close to the experimental value[40]. In all the calculations, one CO molecule is pre-adsorbed on the surface as a spectator and therefore the surface is a 0.25 ML CO pre-covered Co0001 surface.

The climbing image nudged elastic band (CI-NEB) method[41] was used to locate the initial transition states, which were subsequently optimized by using the dimer[42] method. The calculations were converged until all the forces were less than 0.01 eV/Å and the total energy changed less than $10^{-7}$ eV/atom between two successive optimizations. The vibration frequencies were calculated to verify the transition states with one negative mode corresponds to the desired reaction coordinates.

Adsorption energies of surface species and the activation energy of elementary steps were calculated as:

$$E_{ads} = E_{A+slab} - E_A - E_{slab}$$

$$E_a = E_{TS} - E_{IS}$$

where $E_A$ is the total energy of molecule A in the gas phase, $E_{slab}$ is the total energy of 0.25ML CO pre-covered surface or clean surface, $E_{A+slab}$ is the minimum total energy of the surface species on the slab, $E_a$ is the activation energy of elementary step, $E_{TS}$ is the total energy of the transition state and $E_{IS}$ is the total energy of the reactant. Activation energies of bimolecular surface reactions were calculated as the energy difference between the transition state and the reactant co-adsorbed on the surface. Moreover, zero point energies were included in the calculation of activation energy as shown in the following equation:

$$E_{ZPE} = \sum_{i=1}^{3N-6(5)} \frac{N_A h \nu_i}{2},$$

where $N_A$ is Avogadro's number, h is Plank's constant, $\nu_i$ is the frequency of the normal mode and N is the number of atoms.

Isotope effects were accounted for through its contributions to energetics with zero point energy corrections as well as entropies (see details in S1). Moreover, the isotope effect for kinetically relevant steps is described by kinetic isotope effect (KIE), while the quasi-equilibrated steps are represented by equilibrium isotope effect (EIE). For adsorbed species, the frustrated translational and rotational modes are treated as special cases of vibrational modes. Accordingly, the entropy is evaluated by:

$$S = S_{vib} = R \sum_i^{3N} \left( \frac{x_i}{e^{x_i} - 1} - ln(1 - e^{-x_i}) \right),$$

where $x_i = \frac{hc}{k_B T} \frac{1}{\lambda_i}$, c is speed of light, $k_B$ is Boltzmann constant, and $1/\lambda_i$ is the wavenumber corresponding to each vibrational frequency. All the frequencies, including those for spectator CO*, except the imaginary one corresponding to the transition state of each elementary step, were accounted for in all ZPE and entropy calculation. For gas phase of $H_2$, the detailed procedure has been described[19, 23].

The steady-state isotopic transient kinetic analysis as well as kinetic isotopic analysis were performed on a Co (20 wt%)/CNT catalysts. The cobalt particle size is about 18 nm by $H_2$ chemisorption. The kinetic experiments were carried out in a fixed-bed reactor at 483 K, 1.85 bar and $H_2$/CO =3-15. The reaction order of $H_2$ and CO was obtain by varying $H_2$ and CO partial pressure. The kinetic isotopic effect was determined by switching the feed from $H_2$/CO to $D_2$/CO at 483 K, 1.85 bar and $H_2$/CO =10. The catalysts properties and experimental details are reported previously[23].

## 3. Results and discussion

### 3.1 Direct mechanisms of methane formation

A systematic approach to analysis, simplification and reduction of detailed mechanisms of heterogeneous catalytic reactions has been developed based on the theory of reaction routes[43]. A direct overall reaction route is defined as a linear combination of q + 1 selected elementary steps that eliminate all of the q intermediates, thus producing an overall reaction involving only terminal species[44]. It is well-known that the methane formation pathways consist of CO dissociation (i.e., CO direct dissociation and H-assisted dissociation) and the resultant $CH_x$ stepwise hydrogenation, in which different CO dissociation pathways will cause different methane formation pathways[14, 15, 23]. Particularly, the H-assisted CO dissociation route has many different pathways, depending on the number of hydrogen addition before the cleavage of the C-O bond. By considering the above factors, 21 elementary steps are summarized in Table 1. It should be mentioned that the elementary reaction steps listed in Table 1 is only a part of the model for F-T synthesis where the reaction steps of chair growth are not included. Nine carbon pathways for the methane formation were identified from the 21 elementary steps and the pathways are schematically shown in Fig. 1. Furthermore, nine kinds of reaction pathways were expressed into nine types of direct mechanisms of $CH_4$ formation (Table S1), which involved additional gas-phase species adsorption as well as $CH_x$ and $OH_x$ stepwise hydrogenation. The evaluation of nine kinds of direct mechanisms based on energetics, kinetic analysis, and kinetic isotope effect will be carried out in Section 3.2-3.4, aiming at discriminating which one of several kinds of mechanisms are the dominating mechanism.

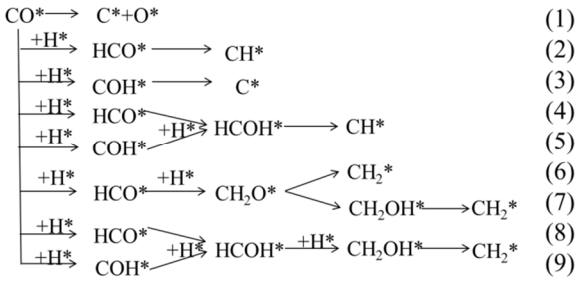


**Fig. 1** Nine kinds of carbon pathways involved in methane formation ($CH_x$ stepwise hydrogenation are not presented for the sake of clarity).

**Table 1** Activation energies of elementary steps in methane formation.

| No | Elementary steps | $E_a$ (eV) | References |
|---|---|---|---|
| $s_1$ | $CO(g) + * \rightarrow CO*$ | - | |
| $s_2$ | $H_2(g) + 2* \rightarrow 2H*$ | 0.53 (0.51) | 0.52[14] |
| $s_3$ | $CO* + * \rightarrow C* + O*$ | 3.37 (3.32) | 3.80[14], 2.28[16],2.82[17] |
| $s_4$ | $CO* + H* \rightarrow COH* + *$ | 1.55 (1.42) | 1.80[45],1.30[14] |
| $s_5$ | $COH* + * \rightarrow C* + OH*$ | 2.68 (2.64) | 3.26[14] |
| $s_6$ | $COH* + H* \rightarrow HCOH* + *$ | 0.79 (0.81) | 0.46[14],0.85[45] |
| $s_7$ | $HCOH* + * \rightarrow CH* + OH*$ | 0.73 (0.65) | 1.10[14] |
| $s_8$ | $HCOH* + H* \rightarrow CH_2OH* + *$ | 0.71 (0.65) | 0.82[45] |
| $s_9$ | $CH_2OH* \rightarrow CH_2* + OH*$ | 0.83 (0.71) | |
| $s_{10}$ | $CO* + H* \rightarrow HCO* + *$ | 1.25 (1.25) | 1.43[14], 1.51[16], 1.31[45] |
| $s_{11}$ | $HCO* + * \rightarrow CH* + O*$ | 0.90 (0.85) | 0.95[14],1.36,0.93[16] |
| $s_{12}$ | $HCO* + H* \rightarrow HCOH* + *$ | 0.80 (0.69) | 0.93[14],1.23[45] |
| $s_{13}$ | $HCO* + H* \rightarrow CH_2O* + *$ | 0.24 (0.26) | 0.15[14],0.55[45], 0.45[17], 0.61[46] |
| $s_{14}$ | $CH_2O* + H* \rightarrow CH_2OH* + *$ | 1.20 (1.08) | 1.27[45] |
| $s_{15}$ | $CH_2O* + * \rightarrow CH_2* + O*$ | 0.95 (0.87) | 1.63[14],0.70[16],1.22[46],0.95[45] |
| $s_{16}$ | $C* + H* \rightarrow CH* + *$ | 0.28 (0.20) | 0.75[47],0.83[48],0.41[14],0.85[10] |
| $s_{17}$ | $CH* + H* \rightarrow CH_2* + *$ | 0.18 (0.14) | 0.37[14],0.65[48],0.66[10] |
| $s_{18}$ | $CH_2* + H* \rightarrow CH_3* + *$ | 0.34 (0.28) | 0.43[47],0.60[48],0.63[10] |
| $s_{19}$ | $CH_3* + H* \rightarrow CH_4(g) + 2*$ | 0.26 (0.23) | 0.88[47],0.96[48],1.09[10] |
| $s_{20}$ | $O* + H* \leftrightarrow OH* + *$ | 0.71 (0.59) | 0.49[14],0.81[46],1.72[17] |
| $s_{21}$ | $OH* + H* \leftrightarrow H_2O + 2*$ | 0.88 (0.77) | 0.64[14],0.46[46],1.42[17] |

All the activation energies are calculated on 0.25 ML CO pre-covered Co(0001) surface. The data in the parentheses are those including ZPE corrections. [14]Co(0001) surface with 0.5 ML CO coverage, PW91 functional by DACAPO ; [12]Co(0001) surface, PBE functional by VASP; [45]Co(0001) surface, PBE functional by SIESTA code; [16]Co(0001) surface, PBE functional by VASP; [49]Co(0001) surface with 1/3 ML CO coverage, PBE functional by VASP; [48]Co(0001) surface, PBE functional by SIESTA; [17]Co(0001) surface, RPBE functional by CASTEP; [10, 46]Co(0001) surface, PW91 functional by CASTEP; [47] Co(0001), PBE functional by SIESTA.

### 3.2 Discrimination of mechanisms based on reaction energetics

#### 3.2.1 Adsorption of surface species

DFT calculations of adsorption configurations and energies of all intermediates involved in the elementary reactions were performed for the surface species on clean Co(0001) surface and 0.25 ML CO pre-covered surface, in which all the most stable structures and the corresponding adsorption energies were summarized in Fig. 2 and Table 2, respectively. The data in the parentheses are calculated on 0.25 ML CO pre-covered Co(0001) surface.

As shown in Fig. 2 and Table 2, CO*, CH*, $CH_2$* and $CH_3$* prefer to adsorb at hollow sites with the C atom bonding to Co and the other atoms pointing outward, which are consistent with previous theoretical studies[10, 12, 39, 46]. Particularly, the adsorption energies of CO*, CH* and $CH_2$* are -1.67, -6.51, and -3.90 eV on 0.25ML CO pre-covered surface, respectively, which are in good agreement with those obtained by Saeys et al..[49] For HCO*, the C atom bonds to two Co atoms, and the O atom binds with another Co atom. However, for $CH_2O$*, the O atom binds with two Co atoms, and the C atom binds with another Co atom. Other surface species, i.e., COH*, HCOH* and $CH_2OH$* adsorb on the surface via carbon atom binding with Co atoms and $OH_x$ pointing outward. The geometries of these oxygenates are consistent with those obtained by Hu et al..[45]

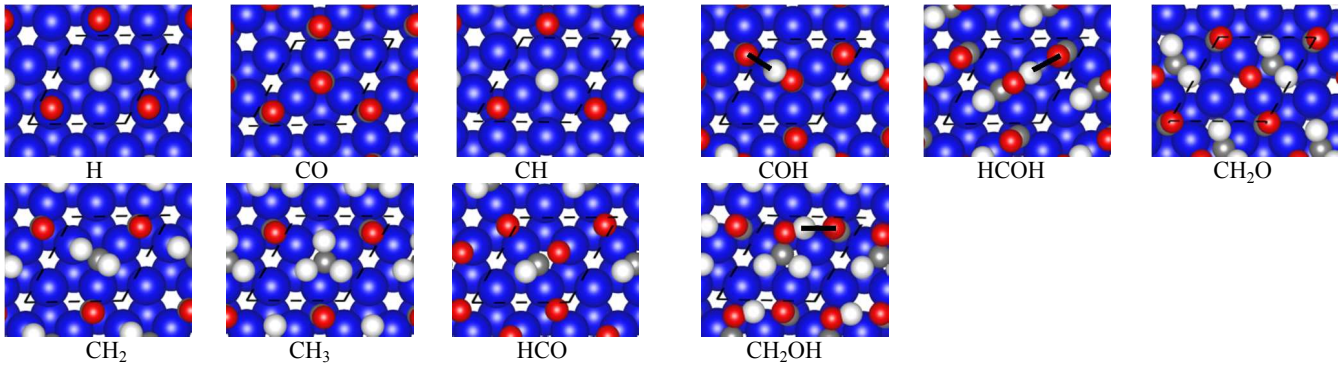


**Fig. 2** The most stable adsorption configurations of main surface species on Co(0001) surface, where the blue balls are cobalt atoms, the gray ones are carbon atoms, the red ones are oxygen atoms, and the white ones are hydrogen atoms. The black solid lines represent hydrogen bonds.

**Table 2** Energetic and geometric properties of main surface species on Co(0001) surface.

| Species | $E_{ads}$ (eV) | $E_{ads}$ (eV) in literature | Geometry |
|---|---|---|---|
| H | -2.85 (-2.60) | ,-2.78[12],-2.90[16],-2.85(-2.61)*[49],-2.88(-2.29)*[14] | fcc |
| CO | -1.70 (-1.67) | -1.64[12], -1.81[16], -1.72 (-1.68)*[49], -1.88 (0.78) *[14] | fcc |
| CH | -6.72 (-6.51) | -6.30[12], -6.46[16], -6.43(-6.22)*[49], -6.31 (-5.48)*[14], -6.54[48] | fcc |
| $CH_2$ | -4.03 (-3.90) | -3.95[12], -4.10[16], -4.03 (-3.93)*[49], -3.86 (-2.73)*[14], -3.86[48] | fcc |
| $CH_3$ | -1.98 (-1.37) | -1.89[12], -2.08[16], -2.00[48] | fcc |
| HCO | -2.17 (-1.93) | -2.14[12], -2.20[45], -2.22[16], -2.24 (0.37)[14] | fcc |
| COH | -4.35 (-4.71) | -4.38[45], -4.38 (-3.37)[14] | fcc |
| HCOH | -2.97 (-2.90) | -3.82[45], -3.00 (-1.92)[14] | hcp |
| $CH_2O$ | -0.82 (-0.30) | -0.86[45], -0.90[16], -0.88 (-0.29)[14] | hcp |
| $CH_2OH$ | -1.56 (-1.00) | -1.72[45] | fcc |

The results were calculated on clean Co(0001) surface and 0.25 ML CO pre-covered surface, respectively, and the data in the parentheses are calculated on 0.25 ML CO pre-covered Co(0001) surface. In addition, the results in the parentheses from literature were also calculated on CO pre-covered surfaces, in which 0.5 ML CO coverage[14], and 1/3 ML CO coverage[49] were employed.

In principle, the pre-covered CO molecule usually decreases the stability of other molecules due to the interaction between the adsorbed species. The destabilization of adsorbed species reflects through-space repulsive interactions with CO. Effects of the interaction on the adsorption heat are stronger for larger molecules[14, 49]. As shown in Table 2, for most surface species, the adsorption energies are smaller on 0.25ML CO pre-covered surface than on a clean surface. Unexpectedly, the adsorption energy of COH* is larger compared with that on the clean surface, which is opposite to what was reported by Iglesia et al.[14]. This might be a result of that the O atom in the pre-covered CO* interacts with the O-H in the COH* to form a hydrogen bond ($d_{O-H}$=1.68Å), which is labelled by solid line in Fig. 2. H-bonding between the adsorbed COH* and CO* obviously stabilizes the adsorption of COH*. Besides, the CO coverage is 0.25ML, which is smaller than that of Iglesia et al. (0.5ML), therefore the repulsive interaction is weaker and the stabilizing effect of a hydrogen bond is relative obvious which may lead to the an increase of the adsorption energy. It is noted that the PBE functional is not a good descriptor for hydrogen bonding, so the BEEF-vdW functional[52] was utilized to further investigate the possible effect of H bond on the adsorption heat. The results confirmed that the adsorption of COH* is stronger on CO pre-covered surface with a difference of 0.34 eV. Such stabilizing effects through H-bonding could exist also for HCOH* and $CH_2OH$*. However, the difference in adsorption energy between the pre-covered CO Co(0001) surface and the clean surface depends on the competition between the destabilizing effect through space repulsive interactions with CO and stabilizing effect through H-binding with CO. The adsorption energies of $CH_2O$* and $CH_2OH$* on the pre-covered CO Co(0001) surface are smaller than those reported on the clean surface (Table 2) possibly as a result of more significant destabilizing effect through space repulsive interactions than stabilizing effect through H-binding, due to their large size.

### 3.2.2 Activation energies of the elementary steps

DFT calculations of activation energies of the elementary steps were also performed on 0.25 ML CO pre-covered Co(0001) surface, and ZPE corrections were included in the activation energies concerning most elementary steps involving hydrogen-containing species [50,51]. The resultant activation energies are presented in Table 1. The corresponding stable configurations and the geometrical parameters of transition states (TS) are shown in Table S2 and Table S3 in supplementary information, respectively. Though the CO coverage, DFT functional and



 

packages employed in the literature are different from our calculations, these literature values are also listed in Table 1 in order to see the apparent trend. It can be seen that the activation energies obtained in the present work are rather consistent with previous theoretical values except for the reaction steps of $CH_x$ hydrogenation[10, 15, 39, 45-49]. The activation energies for $CH_x$ (x=0-3) hydrogenation steps (Table 1) are smaller than literature values, which might be a result of the reduced adsorption strength of $CH_x$ due to the fact that co-adsorption of CO molecules on the surface decreases the energy barrier of bond formation reactions. The activation energy of 0.62eV, 0.55eV, 0.46eV, 0.87eV for $CH_x$ hydrogenation were obtained on clean surface for x from 1 to 3, respectively. These values were found to be comparable with the literature values without CO co-adsorption. Moreover, the co-adsorbed $CH_x$+H was taken as the initial state (reactant), which typically results in around 0.3eV less compared to the values obtained from $CH_x$ and H individually adsorbed on the surface, according to the results from Hu et al[10].

Combining the values of activation energies with the analysis of the direct mechanisms of methane formation in Section 3.1, nine kinds of complete direct reaction mechanisms (Table S1) would be further expressed as the following sequence of elementary steps:

$M_1$. {$s_1$, $3s_2$, $s_3$, $s_{16}$, $s_{17}$, $s_{18}$, $s_{19}$, $s_{20}$, $s_{21}$}
$M_2$. {$s_1$, $3s_2$, $s_{10}$, $s_{11}$, $s_{17}$, $s_{18}$, $s_{19}$, $s_{20}$, $s_{21}$}
$M_3$. {$s_1$, $3s_2$, $s_4$, $s_5$, $s_{16}$, $s_{17}$, $s_{18}$, $s_{19}$, $s_{21}$}
$M_4$. {$s_1$, $3s_2$, $s_{10}$, $s_{12}$, $s_7$, $s_{17}$, $s_{18}$, $s_{19}$, $s_{21}$}
$M_5$. {$s_1$, $3s_2$, $s_4$, $s_6$, $s_7$, $s_{17}$, $s_{18}$, $s_{19}$, $s_{21}$}
$M_6$. {$s_1$, $3s_2$, $s_{10}$, $s_{13}$, $s_{15}$, $s_{18}$, $s_{19}$, $s_{20}$, $s_{21}$}
$M_7$. {$s_1$, $3s_2$, $s_{10}$, $s_{13}$, $s_{14}$, $s_9$, $s_{18}$, $s_{19}$, $s_{21}$}
$M_8$. {$s_1$, $3s_2$, $s_{10}$, $s_{12}$, $s_8$, $s_9$, $s_{18}$, $s_{19}$, $s_{21}$}
$M_9$. {$s_1$, $3s_2$, $s_4$, $s_6$, $s_8$, $s_9$, $s_{18}$, $s_{19}$, $s_{21}$}

To compare different steps involved in different mechanisms more clearly, the activation energies for each elementary step ($s_i$) are displayed in corresponding matrixes as above. Accordingly, the activation energies for these direct mechanisms are:

$M_1$. {0, 0.51, 3.32, 0.20, 0.14, 0.28, 0.23, 0.59, 0.77}
$M_2$. {0, 0.51, 1.25, 0.85, 0.14, 0.28, 0.23, 0.59, 0.77}
$M_3$. {0, 0.51, 1.42, 2.64, 0.20, 0.14, 0.28, 0.23, 0.77}
$M_4$. {0, 0.51, 1.25, 0.69, 0.65, 0.14, 0.28, 0.23, 0.77}
$M_5$. {0, 0.51, 1.42, 0.81, 0.65, 0.14, 0.28, 0.23, 0.77}
$M_6$. {0, 0.51, 1.25, 0.26, 0.87, 0.28, 0.23, 0.59, 0.77}
$M_7$. {0, 0.51, 1.25, 0.26, 1.08, 0.71, 0.28, 0.23, 0.77}
$M_8$. {0, 0.51, 1.25, 0.69, 0.65, 0.71, 0.28, 0.23, 0.77}
$M_9$. {0, 0.51, 1.42, 0.81, 0.65, 0.71, 0.28, 0.23, 0.77}

The number in the above matrixes represents corresponding activation energy of the step ($s_i$), and the unit is eV.

It can be observed that the highest energy barriers for $M_1$ (3.32 eV) and $M_3$ (2.64 eV) are much higher than other reaction mechanisms. For $M_1$, the highest energy barriers is the step $s_3$ (i.e., the CO* decomposition in CO direct dissociation mechanism), while for $M_3$, it is the step $s_5$ (i.e., the COH* decomposition). Though the reaction rate depends not only the rate constant but also the concentration of the surface species, these two direct mechanisms can be excluded, as a result of that $M_1$ and $M_3$ reaction routes are energetically very unfavorable compared to other reaction routes. The steps with the highest energy barriers in the mechanism of $M_1$ and $M_3$ reflect the dissociation of CO (step $s_3$, 3.32 ev) and COH (step $s_5$, 2.64 ev), respectively. These energy barriers are much higher than the dissociation of HCO (step $s_{11}$, 0.85 ev). To understand the dependence of energy barriers of C-O cleavage on the molecule structure, the geometrical properties of CO*, HCO* and COH* are investigated and compared. The bond lengths of C-O in HCO* (1.30 Å) and COH* (1.31 Å) are longer than that of C-O in CO* (1.19 Å) (Table S2). Clearly, the C-O bonds in HCO* and COH* are suggested to be pre-activated by CO hydrogenation and sharply weaken the C-O bond strength. This explains well that the hydrogen assisted CO activation is more energetically favorable compared to the direct CO dissociation. On the other hand, HCO* bonds to the surface through C and O atoms, while COH* bonds to the surface only through carbon atom. Both bonding of C and O with Co surface sites in HCO obviously destabilizes the adsorption of HCO (-1.93 eV, Table 2), compared to the adsorption of COH (-4.71 eV, Table 2). As a consequence, such adsorption configuration of HCO promotes the cleavage of the C-O bond in step $s_{11}$ (HCO*+*→CH*+O*, 0.85 eV) compared to step $s_5$ (COH*+*→C*+OH*, 2.64 eV). This explains well the higher energy in $M_3$ than the one in $M_2$.

Based on the above analyses, it can be concluded that CO direct dissociation (i.e., $M_1$) and COH dissociation ($M_3$) are energetically unfavorable on Co(0001) surface, consistent with previous results[14, 16, 19, 23]. The contribution of reaction routites of $M_1$ and $M_3$ to the reaction can be ignored. Moreover, for H-assisted CO dissociation via HCO* and COH* intermediates, $M_2$, $M_4$, and $M_5$ direct mechanisms are energetically more favorable than $M_6$, $M_8$ and $M_9$ mechanisms. However, it is not possibly to discriminate these reaction routes only based on activation analysis since reaction rate depends on both the rate constant and concentrations.

### 3.2.3 Discrimination of reaction mechanisms based on free energy

To compare the other reaction pathways at the same level, the free energy profiles for all the mechanisms except for $M_1$ and $M_3$ are displayed in Fig.S1 in supplementary information, where the adsorbed CO and 6H ($CO+3H_2$), as well as a co-adsorb CO molecule were used as the reference state setting as a zero free energy. The steps for $CH_x$ hydrogenation and $H_2O$ formation are common for all reaction routes. The difference is mainly on the free energy for different steps for CO activation and decomposition of hydrogenated intermediates. The details for the calculations of the free energy at reaction temperature of 483K are elucidated in supporting information S2 and can be found in previous literature[53]. In order to clearly elucidate the different pathways, the effective barriers ($E_{eff}$), which is the difference in free energy between the highest energy and the reference state adsorbed 6H*+2CO* for different reaction pathways, are shown in Fig. S1. The results indicated that the effective barriers of all the mechanisms expect $M_7$ are the same with 2.56 eV. A higher effective barrier of 2.85 eV was found for the mechanism $M_7$, indicating that $M_7$ is energetically less favorable than others. However, the free energy for several elementary steps in $M_2$, $M_4$, $M_5$, $M_6$, $M_8$, and $M_9$ are rather close, and it is difficult to discriminate these reaction routes only based on the free energy profiles. Discrimination of these reaction routes are further performed based on kinetic and kinetic isotope effect analysis in the following sections.

Journal Name RSCPublishing

ARTICLE

### 3.3 Discrimination of mechanisms based on kinetic analysis

Although kinetic analysis cannot be used to exclusively elucidate the mechanism, it can be used to exclude some proposed mechanisms. We have employed kinetic analysis to discriminate the remaining six kinds of direct mechanisms ($M_2$, $M_4$, $M_5$, $M_6$, $M_8$ and $M_9$) by comparing the reaction orders of derived Langmuir-Hinshelwood (L-H) rate expressions with our previous results from SSITKA experiments. COH* and HCO* as well as HCOH* and $CH_2O$* give the same L-H equations; hence it is difficult to distinguish between them in a kinetic analysis. Therefore, the remaining six kinds of mechanisms can be simplified to the following four typed mechanisms:

Type I: $M_2$

$CO + * \leftrightarrow CO*$ [1]
$H_2 + 2* \leftrightarrow 2H*$ [2]
$CO* + H* \leftrightarrow HCO* + *$ [3]
$HCO* + * \rightarrow CH* + O*$ [4]
$CH* + H* \leftrightarrow CH_2*$
$CH_2* + H* \leftrightarrow CH_3*$
$CH_3* + H* \leftrightarrow CH_4 + *$
.....
$O* + H* \leftrightarrow OH* + *$
$OH* + H* \leftrightarrow H_2O + 2*$

Type II: $M_4$ (or $M_5$)

$CO + * \leftrightarrow CO*$ [1]
$H_2 + 2* \leftrightarrow 2H*$ [2]
$CO* + H* \leftrightarrow HCO* + *$ [3]
$HCO* + H* \leftrightarrow HCOH* + *$ [4]
$HCOH* + * \leftrightarrow CH* + OH*$ [5]
$CH* + H* \leftrightarrow CH_2*$
$CH_2* + H* \leftrightarrow CH_3*$
$CH_3* + H* \leftrightarrow CH_4 + *$
.....
$OH* + H* \leftrightarrow H_2O + 2*$

Type III: $M_6$

$CO + * \leftrightarrow CO*$ [1]
$H_2 + 2* \leftrightarrow 2H*$ [2]
$CO* + H* \leftrightarrow HCO* + *$ [3]
$HCO* + H* \leftrightarrow CH_2O* + *$ [4]
$CH_2O* + * \rightarrow CH_2* + O*$ [5]
$CH_2* + H* \leftrightarrow CH_3*$
$CH_3* + H* \leftrightarrow CH_4 + *$
.....
$O* + H* \leftrightarrow OH* + *$
$OH* + H* \leftrightarrow H_2O + 2*$

Type IV: $M_8$ (or $M_9$)

$CO + * \leftrightarrow CO*$ [1]
$H_2 + 2* \leftrightarrow 2H*$ [2]
$CO* + H* \leftrightarrow HCO* + *$ [3]
$HCO* + H* \leftrightarrow HCOH* + *$ [4]
$HCOH* + H* \rightarrow CH_2OH* + *$ [5]
$CH_2OH* + * \leftrightarrow CH_2* + OH*$ [6]
$CH_2* + H* \leftrightarrow CH_3*$
$CH_3* + H* \leftrightarrow CH_4 + *$
.....
$OH* + H* \leftrightarrow H_2O + 2*$

In our previous work, the step $s_{12}$: HCO*+H*↔HCOH*+*, has been identified as a kinetically relevant step for CO activation by combined kinetic and isotopic kinetic effect analysis[23]. Although the activation energy of the step CO*+H*↔HCO*+* is higher compared to the steps HCO*+H→HCOH*+* or HCOH*+*↔CH*+OH*. The step HCO*+H*↔HCOH*+* was found to be the rate-determining step (RDS), suggesting an important effect of the coverage. The site coverage of CO* and H* are much higher than HCO* and HCOH*. The reaction order with respect to $H_2$ and CO has been determined to be 0.55 and -0.35 for CO activation, respectively and 0.64 and -0.65 for methane formation, respectively. It suggests that the rate determining step or steps are not identical for CO activation and methane formation. The global reaction order for CO conversion with respect to $H_2$ and CO was found to vary between 0.5-0.8 and -0.6 to -0.2, respectively for cobalt based catalysts at 20 bar and $H_2$/CO=2.5 tested in a CSTR reactor[54]. The reaction orders found in our study (methanation condition) are in the same range as found at real Fischer-Tropsch conditions. This suggests that the conclusion drawn in our study is relevant for FTS. However, a full kinetic model including chain growth and termination is necessary in order to describe selectivity in Fischer-Tropsch synthesis.

For type I (i.e., $M_2$), a kinetic analysis cannot distinguish between the step [3] or [4] as the RDS, since they have an identical rate expression (Table 3). The global reaction order of hydrogen ($n_{H2}$) depends on the intrinsic reaction order ($n_{int.H2}$) and the hydrogen site coverage as shown in the following equation:

$$n_{H_2} = n_{int,H_2} - \theta_H$$

The reaction order with respect to hydrogen of 0.64 suggests that the reaction steps before the RDS could involve about 2 hydrogen atoms, an intrinsic $H_2$ reaction order of 1. Applying this criteria, for type II (i.e., $M_4$ and $M_5$), the step HCO*+H*→HCOH*+* or HCOH*+*↔CH*+OH* is assumed as a RDS. For type III (i.e., $M_6$), the step HCO*+H*→$CH_2O$*+* or $CH_2O$*+*→$CH_2$*+O* is assumed as RDS, and for type IV (i.e., $M_8$ and $M_9$), the step HCOH*+H*→$CH_2OH$*+* or $CH_2OH$*+*↔$CH_2$*+OH* is assumed as RDS. The Langmuir-Hinshelwood (LH) rate expressions for methane formation were derived (see details in S2) based on the assumed RDS and the expressions are summarized in Table 3.

Table 3 shows that the reaction orders for CO are almost identical for different direct mechanisms, while those for $H_2$, reflecting the number of H involved in both RDS and the steps before RDS, are sensitive to the type of direct mechanisms. As shown in Table 3, the reaction order for $H_2$ in type I (i.e., $M_2$) could vary from 0.5 at zero hydrogen site coverage and to -0.5

at the site coverage of hydrogen of 1. The typical site coverage of hydrogen was experimentally found in the range of 0.1 to 0.35 at the conditions studied[23]. Obviously it does not match our experimental reaction order of $H_2$ (0.64). Therefore, $M_2$ direct mechanism can be excluded according to the kinetic analysis. The intrinsic reaction order with respect to hydrogen in $M_8$ (or $M_9$) is 1.5 (type IV in Table 3). As a result, the global hydrogen order could not fit well with the experimental reaction order of hydrogen, and therefore the mechanisms $M_8$ and $M_9$ can be excluded. Both type II and III models, corresponding to $M_4$, $M_5$, and $M_6$ (Table 3), respectively, fit well the experimental data. However, $M_4$, $M_5$, and $M_6$ have similar rate expression, which cannot be distinguished by kinetic analysis only.

**Table 3** The reaction order for $H_2$ and CO in different pathways

| Type | Mechanisms | Rate expression | reaction order for $H_2$ | | reaction order for CO | |
|---|---|---|---|---|---|---|
| | | | cal | exp[23] | cal | exp[23] |
| I | $M_2$ | $r = \frac{k_4 K_3 K_{CO} P_{CO} \sqrt{K_{H_2} P_{H_2}}}{\left(1 + \sqrt{K_{H_2} P_{H_2}} + K_{CO} P_{CO}\right)^2}$ | (-0.5,0.5) | | (-1,1) | |
| II | $M_4$(or $M_5$) | $r = \frac{k_5 K_4 K_3 K_{CO} K_{H_2} P_{CO} P_{H_2}}{\left(1 + K_{CO} P_{CO} + \sqrt{K_{H_2} P_{H_2}}\right)^2}$ | (0,1) | 0.64 | (-1,1) | -0.65 |
| III | $M_6$ | $r = \frac{k_5 K_4 K_3 K_{CO} K_{H_2} P_{CO} P_{H_2}}{\left(1 + \sqrt{K_{H_2} P_{H_2}} + K_{CO} P_{CO}\right)^2}$ | (0,1) | | (-1,1) | |
| IV | $M_8$(or $M_9$) | $r = \frac{k_6 K_5 K_4 K_3 K_{CO} P_{CO} \left(K_{H_2} P_{H_2}\right)^{1.5}}{\left(1 + \sqrt{K_{H_2} P_{H_2}} + K_{CO} P_{CO}\right)^2}$ | (0.5,1.5) | | (-1,1) | |

### 3.4 Discrimination of mechanisms based on kinetic isotope effect analysis

The kinetic isotope effect (KIE) is defined as the ratio of rates with $CO/H_2$ and $CO/D_2$ as reactants, and it is a versatile tool to elucidate reaction mechanisms and the nature of transition states. At 483 K, 1.85 bar and $H_2/CO$ =10 from our previous SSITKA results[23], the overall KIE values for CO conversion and methane formation were 0.78 and 0.99, respectively. In addition to the difference in the reaction order between CO activation and methane formation, the KIE results suggest different kinetically relevant steps involved in the methane formation compared with CO activation. The isotopic effect measures the difference in rate constants for the RDSs and in the equilibrium constants for the equilibrated steps involving specific intermediates that contain deuterium and hydrogen isotopomers[19]. For the rate constant, the pre-exponential factor (A) is represented by the entropy difference between hydrogen and deuterium isotopomers, and the activation energy with ZPE correction are utilized. Moreover, the kinetic isotope effect (KIE) accounts for the entropy and zero point energy differences between the initial state (IS) and the transition state (TS), while the equilibrium isotope effect (EIE) accounts for the differences between the initial state (IS) and final state (FS) in the elementary steps.

As mentioned above, all the zero point energies and entropies can be calculated by vibrational frequencies, and the frequencies are shown in Table S4 in supplementary information. It is commonly accepted that the heavier D-atom decreases the vibrational frequencies. Based on the ZPE and entropies of all the ISs, TSs and FSs, the KIE and EIE values for relevant elementary steps were calculated, and the results were summarized in Table 4. It can be seen that the EIE values for $H_2$+2*→H*+H*, CO*+H*→COH* and CO*+H*→HCO* are 0.61, 0.63 and 0.62, respectively and the KIE value for HCO *+H*→HCOH* is 1.98, which are consistent with the results from Iglesia et al.[19]. However, the KIE for COH*+H*→HCOH* is different from their results due to the hydrogen bond formation between the O atom in CO and the O-H atoms in COH which has been mentioned above. Moreover, the EIE values are observed to be less than 1 for those elementary steps with the hydrogen atom involved in the bond-breaking and formation, such as CO*+H* → HCO* and HCO*+H* → HCOH*+*. However, the KIE and EIE values are around 1 for these steps in which the hydrogen atom is not involved in the bond-breaking and formation, such as COH*+*→C*+OH* and HCOH*+*→CH*+OH*.

**Table 4** Equilibrium isotope effect (EIE) and kinetic isotope effect (KIE) for relevant elementary steps

| No | Elementary steps | EIE | KIE |
|---|---|---|---|
| $s_2$ | $H_2$ (g) + 2* → 2H* | 0.61 (0.61)[19] | - |
| $s_4$ | CO* + H* → COH* + * | 0.63 (0.64)[19] | 0.60 |
| $s_5$ | COH* + * → C* + OH* | 0.94 | 0.88 |
| $s_6$ | COH* + H* → HCOH* + * | 0.49 | 0.69 (1.24)[19] |
| $s_7$ | HCOH* + * → CH* + OH* | 1.11 | 1.02 |
| $s_8$ | HCOH* + H* → $CH_2OH$* + * | 0.57 | 1.66 |
| $s_9$ | $CH_2OH$* → $CH_2$* + OH* | 1.20 | 1.27 |
| $s_{10}$ | CO* + H* → HCO* + * | 0.62 (0.64)[19] | - |
| $s_{11}$ | HCO* + * → CH* + O* | 1.02 | 1.01 |
| $s_{12}$ | HCO* + H* → HCOH* + * | 0.58 | 1.98 (1.79)[19] |
| $s_{13}$ | HCO* + H* → $CH_2O$* + * | 0.61 | 0.86 |
| $s_{14}$ | $CH_2O$* + H* → $CH_2OH$* + * | 0.57 | 2.22 |
| $s_{15}$ | $CH_2O$* + * → $CH_2$* + O* | 1.04 | 1.12 |
| $s_{16}$ | C* + H* → CH* + * | 0.59 | 1.79 |
| $s_{17}$ | CH* + H* → $CH_2$* + * | 0.67 | 1.62 |
| $s_{18}$ | $CH_2$* + H* → $CH_3$* + * | 0.57 | 1.69 |
| $s_{19}$ | $CH_3$* + H* → $CH_4$(g) + 2* | - | 1.55 |

The kinetic isotope effects for the remaining mechanism $M_4$, $M_5$ and $M_6$ were further calculated in order to discriminate between the mechanisms. In these mechanisms, one or several kinetically relevant steps may be involved. Each step was first assumed as the rate determining step (RDS), and the steps before RDS were equilibrated. Afterwards, the overall KIE of these mechanisms were calculated, in which KIE was employed for RDS and EIE for other steps. Fig. 3 shows the corresponding overall KIE value by assuming each step as RDS. All the estimated KIEs in $M_5$ via the intermediate COH* are much lower than the experimental KIE for CO activation (0.75) and methane formation (0.99). It can therefore be concluded that $M_5$ is the unfavorable reaction route based on the kinetic isotope effect analysis. For the reaction routes $M_4$ and $M_6$ through HCO* intermediate, the overall kinetic isotope effect values for $M_4$ is 0.75, when assuming HCO*+H*→HCOH*+* as RDS. It is consistent with the experimental KIE value (i.e., 0.78) of CO conversion. However, all the KIEs in $M_6$ are also much lower than the experimental values, which is unlikely the dominating reaction routes for the CO activation and the methane formation.

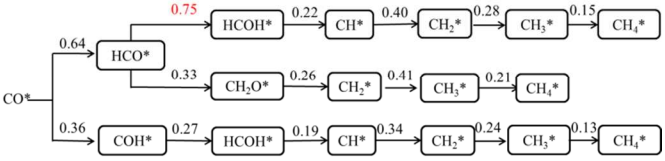


**Fig. 3** The overall kinetic isotope effect (KIE) for reaction $M_4$, $M_6$ and $M_5$ (from top to bottom), respectively, where the values are shown on the assumed RDS.

Since the KIE values for $M_5$ and $M_6$ are far from the experimental value, it can be concluded that $M_4$ is more favorable. $M_4$ proceeds by the H-assisted CO dissociation by HCO* followed by its further hydrogenation into HCOH*. In other words, the H-assisted CO dissociation by HCO* intermediates is the dominating mechanism, which is consistent with previous results[19, 23].

However, the estimated overall KIE values of 0.75 are not consistent with the experimental result of $CH_4$ formation (i.e., 0.99). It should be noted that the analysis so far has been based on the assumption of one RDS in each reaction route. The step of hydrogenation of HCO* into HCOH in $M_4$ has been identified as the RDS for CO activation[23]. Anyhow, the possibility that two or more steps coexist as kinetically relevant steps for methane formation, instead of a single RDS cannot be simply excluded. Based on this assumption, the overall KIE values were reinvestigated, where the step of HCO* hydrogenation was fixed as one of the kinetically relevant steps, and an additional step was assumed to be also the kinetically relevant step. In this way, the corresponding overall KIE values are shown in Fig. 4 where each step was assumed as RDS. The results suggest that the reaction route $M_4$ with two kinetically relevant steps, where the overall KIE values are around 1, is in good agreement with the experimental KIE of $CH_4$ formation (i.e., 0.99). Both steps such as HCO*+H*→HCOH*+* and $CH_2$*+H*→$CH_3$*+* could be the kinetically relevant steps in $M_4$. The hydrogenation of $CH_2$* are the second kinetically relevant step in the reaction route.


**Fig. 4** The overall kinetic isotope effect (KIE) for $M_4$, where HCO*+H*→HCOH* is assumed to be an irreversible step and another step is assumed to be RDS.

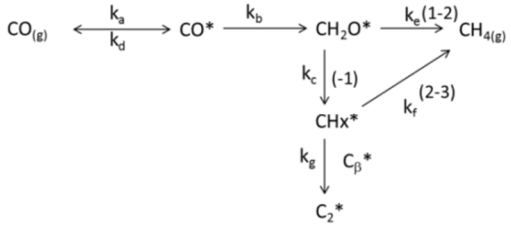


**Fig. 5** The possible reaction scheme and reaction order for methane formation based on kinetic modelling[23]. The number in the parentheses is the reaction order for hydrogen atom.

Transient kinetic methods using SSITKA have been developed which allows us to study methane formation in terms of carbon pools and the number of hydrogen atoms required for methane formation until RDSs[23]. The results are represented in Fig. 6 where the reaction order of hydrogen atom in different steps is shown in the parentheses. It was impossible to distinguish the carbon pool ($C_\alpha$) being $CH_2O$ or HCOH. However, the results of DFT and KIEs suggest HCOH to be the preferred carbon pool in F-T synthesis. HCOH* decomposition leads to the formation of CH*, which could be the carbon pool $C_\beta$. However, the other route shown in Fig. 6 is $M_8$, which is not very favorable based on the kinetic analysis. In the reaction route of direct HCOH* decomposition ($M_4$), two hydrogen atoms are required from HCOH to the RDS ($CH_2$* hydrogenation). It is in good agreement with the reaction order of 2-3 for $k_f$ in Fig. 5.

## 4. Conclusions

We have demonstrated that the combined approach of DFT, kinetic analysis and KIE as a powerful method to discriminate the possible mechanisms for complex reaction systems. Nine kinds of direct mechanisms of methane formation from CO hydrogenation were suggested based on suggested 21 elementary reaction steps. Based on the analysis of activation and free energies from DFT calculations, six kinds of direct mechanisms (i.e., $M_2$, $M_4$, $M_5$, $M_6$, $M_8$ and $M_9$) were suggested as relatively favorable steps. Subsequently, three kinds of direct mechanisms (i.e., $M_2$, $M_8$ and $M_9$) were excluded by comparing the theoretical reaction order from the L-H expressions with the experimental results. Finally, one mechanism was suggested as the dominating reaction route by the analysis of kinetic isotope effects (KIE). As a result, DFT calculation, steady-state kinetic analysis, transient kinetic analysis and kinetic isotope effect analysis consistently support the following reaction route for methane formation from CO hydrogenation on Co catalysts:

CO* undergoes the stepwise hydrogenation to form HCOH*, and the resultant HCOH* is dissociated into CH*. The CH* further undergoes the stepwise hydrogenation to form $CH_4$, in which both the HCO* hydrogenation step and the $CH_2$* hydrogenation step are kinetically relevant steps for methane formation.

## Acknowledgements

The financial support from The Norwegian Research Council through ISP program is gratefully acknowledged. The computational time provided by the Notur project is highly acknowledged.

## Notes and references

[a] Department of Chemical Engineering, Norwegian University of Science and Technology, Sem Sælands vei 4, N-7491 Trondheim, Norway
[b] SINTEF Materials and Chemistry, N-7463 Trondheim, Norway
[c] State Key Laboratory of Chemical Engineering, East China University of Science and Technology, Shanghai 200237, China

Electronic Supplementary Information (ESI) available: [S1. The formulas for KIE calculation, Table S1: A complete list of all the direct reaction mechanisms. Table S2: Geometric information of the species in elementary steps. Table S3: Structure information of the transition states for the elementary steps. Table S4: Vibrational frequencies for the adsorbed species in elementary steps. S2: The details for the calculations of the free energy. S3: Derivation of rate expressions for different mechanisms. Table S5: Chemisorption energies of CO, atomic H and COH at different unit cell size]. See DOI: 10.1039/b000000x/

1 P. Biloen and W. M. H. Sachtler, *Adv. Catal.*, 1981, **30**, 165.
2 G. W. Huber, S. Iborra and A. Corma, *Chem. Rev.*, 2006, **106**, 4044.
3 E. van Steen and M. Claeys, *Chem. Eng. Technol*, 2008, **31**, 655.
4 J. Yang, E. Z. Tveten, D. Chen and A. Holmen, *Langmuir*, 2010, **26**, 16558.
5 J. P. den Breejen, P. B. Radstake, G. L. Bezemer, J. H. Bitter, V. Froseth, A. Holmen and K. P. de Jong, *J. Am. Chem. Soc.*, 2009, **131**, 7197.
6 O. Borg, S. Erib, E. A. Blekkan, S. Storsaeter, H. Wigum, E. Rytter and A. Holmen, *J. Catal.*, 2007, **248**, 89.
7 G. L. Bezemer, J. H. Bitter, H. Kuipers, H. Oosterbeek, J. E. Holewijn, X. D. Xu, F. Kapteijn, A. J. van Dillen and K. P. de Jong, *J. Am. Chem. Soc.*, 2006, **128**, 3956.
8 A. Y. Khodakov, A. Griboval-Constant, R. Bechara and V. L. Zholobenko, *J. Catal.*, 2002, **206**, 230.
9 J. Yang, G. Jacobs, T. Jermwongratanachai, V. R. R. Pendyala, W. P. Ma, D. Chen, A. Holmen and B. H. Davis, *Catal. Lett.*, 2014, **144**, 123.
10 X. Q. Gong, R. Raval and P. Hu, *J. Chem. Phys.*, 2005, **122**.
11 J. Cheng, P. Hu, P. Ellis, S. French, G. Kelly and C. M. Lok, *The J. Phys. Chem. C.*, 2009, **113**, 8858.
12 J. X. Liu, H. Y. Su and W. X. Li, *Catal. Today*, 2013, **215**, 36.
13 M. C. Valero and P. Raybaud, *Catal. Lett.*, 2013, **143**, 1.
14 M. Ojeda, R. Nabar, A. U. Nilekar, A. Ishikawa, M. Mavrikakis and E. Iglesia, *J. Catal.*, 2010, **272**, 287.
15 S. Shetty and R. A. van Santen, *Phys. Chem. Chem. Phys.*, 2010, **12**, 6330.
16 M. K. Zhuo, K. F. Tan, A. Borgna and M. Saeys, *J. Phys. Chem. C.*, 2009, **113**, 8357.
17 O. R. Inderwildi, S. J. Jenkins and D. A. King, *J. Phys. Chem. C.*, 2008, **112**, 1305.
18 C. F. Huo, Y. W. Li, J. G. Wang and H. J. Jiao, *J. Phys. Chem. C.*, 2008, **112**, 3840.
19 M. Ojeda, A. W. Li, R. Nabar, A. U. Nilekar, M. Mavrikakis and E. Iglesia, *J. Phys. Chem. C.*, 2010, **114**, 19761.
20 L. C. Grabow, A. A. Gokhale, S. T. Evans, J. A. Dumesic and M. Mavrikakis, *J. Phys. Chem. C.*, 2008, **112**, 4608.
21 S. L. Shannon and J. G. Goodwin, 1995.
22 H. A. J. van Dijk, J. H. B. J. Hoebink and J. C. Schouten, *Top. Catal.*, 2003, **26**, 111.
23 J. Yang, Y. Qi, J. Zhu, Y.-A. Zhu, D. Chen and A. Holmen, *J. Catal.*, 2013, **308**, 37.
24 M. K. Gnanamani, G. Jacobs, W. D. Shafer and B. H. Davis, *Catal. Today*, 2013, **215**, 13.
25 L. Braconnier, E. Landrivon, I. Clemencon, C. Legens, F. Diehl and Y. Schuurman, *Catal. Today*, 2013, **215**, 18.
26 H. Karaca, O. V. Safonova, S. Chambrey, P. Fongarland, P. Roussel, A. Griboval-Constant, M. Lacroix and A. Y. Khodakov, *J. Catal.*, 2011, **277**, 14.
27 V. O'Shea, N. Homs, J. L. G. Fierro and P. R. de la Piscina, *Catal. Today*, 2006, **114**, 422.
28 D. I. Enache, B. Rebours, M. Roy-Auberger and R. Revel, *J. Catal.*, 2002, **205**, 346.
29 O. Ducreux, J. Lynch, B. Rebours, M. Roy and P. Chaumette, Stud. Surf. Sci. Catal.. 1998, 119, 125.
30 A. Tuxen, S. Carenco, M. Chintapalli, C.-H. Chuang, C. Escudero, E. Pach, P. Jiang, F. Borondics, B. Beberwyck, A. P. Alivisatos, G. Thornton, W.-F. Pong, J. Guo, R. Perez, F. Besenbacher and M. Salmeron, *J. Am. Chem. Soc.*, 2013, **135**, 2273.
31 Z. J. Wang, Z. Yan, C. J. Liu and D. W. Goodman, *Chemcatchem*, 2011, **3**, 551.
32 G. Kresse and J. Hafner, *Phys. Rev. B.*, 1993, **47**, 558.
33 G. Kresse and J. Hafner, *Phys. Rev. B.*, 1994, **49**, 14251.
34 G. Kresse and J. Furthmuller, *Comput. Mater. Sci.*, 1996, **6**, 15.
35 G. Kresse and J. Furthmuller, *Phys. Rev. B.*, 1996, **54**, 11169.
36 Y. A. Zhu, Y. C. Dai, D. Chen and W. K. Yuan, *J. Mol. Cata. a-Chemical*, 2007, **264**, 299.
37 J. P. Perdew, K. Burke and M. Ernzerhof, *Phys. Rev. Lett.*, 1996, **77**, 3865.
38 P. E. Blöchl, *Phys. Rev. B.*, 1994, **50**, 17953.
39 Q. F. Ge and M. Neurock, *J. Phys. Chem. B*, 2006, **110**, 15368.
40 F. Vincent and M. Figlarz, *Seances Academy of Science C*, 1967, **264**, 1270.
41 G. Henkelman, B. P. Uberuaga and H. Jónsson, *J. Chem. Phys.*, 2000, **113**, 9901.
42 G. Henkelman and H. Jonsson, *J. Chem. Phys.*, 1999, **111**, 7010.
43 I. Fishtik and R. Datta, *Surf. Sci.*, 2002, **512**, 229.
44 I. Fishtik, A. Alexander and R. Datta, *Surf. Sci.*, 1999, **430**, 1.
45 J. Cheng, P. Hu, P. Ellis, S. French, G. Kelly and C. M. Lok, . *Phys. Chem. C.*, 2008, **112**, 9464.
46 C. F. Huo, Y. W. Li, J. G. Wang and H. J. Jiao, *J J. Phys. Chem. C.*, 2008, **112**, 14108.
47 J. Cheng, P. Hu, P. Ellis, S. French, G. Kelly and C. M. Lok, *J. Phys. Chem. C.*, 2010, **114**, 1085.
48 J. Cheng, X. Q. Gong, P. Hu, C. M. Lok, P. Ellis and S. French, *J. Catal.*, 2008, **254**, 285.
49 M. K. Zhuo, A. Borgna and M. Saeys, *J. Catal.*, 2013, **297**, 217.

50 R. S. Grev, C. L. Janssen and H. F. Schaefer, *J. Chem. Phys.*, 1991, **95**, 5128.
51 A. Govender, D. C. Ferre and J. W. Niemantsverdriet, *Chemphyschem*, 2012, **13**, 1591.
52 J. Wellendorff, K. T. Lundgaard, A. Mogelhoj, V. Petzold, D. D. Landis, J. K. Norskov, T. Bligard, and K. W. Jacobsen, *Phys. Rev. B.*, 2012, 85, 235149.
53 Y.A. Zhu, D. Chen, X.G. Zhou, W.K. Yuan, Catal. Today, 2009, 148, 260-267.
54 W. Ma, G. Jacobs, D.E. Sparks, M.K. Gnanamani, V.R.R. Pendyala, C.H. Yen, J.L.S. Klettlinger, T.M. Tomsik, B.H. Davis, Fuel, 2010, 90, 756-765.

$$CO^* \xrightarrow{+H} HCO^* \xrightarrow{+H} HCOH^* \longrightarrow CH^* \xrightarrow{+H} CH_2^* \xrightarrow{+H} CH_3^* \xrightarrow{+H} CH_4(g)$$

$$\frac{k_H}{k_D} = \frac{A_H}{A_D}\frac{\Omega_H}{\Omega_D}$$

**KIE** ✚ **DFT**

$$\frac{K_{eq}^H}{K_{eq}^D} = \left[\frac{K_{eq}^H}{K_{eq}^D}\right]^{ZPE} \bullet \left[\frac{K_{eq}^H}{K_{eq}^D}\right]^{S}$$

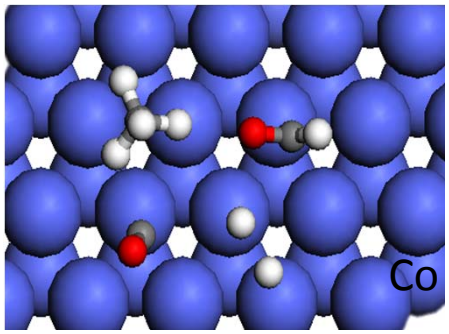


✚ **Kinetic analysis**

$$r = \frac{k_5 K_4 K_3 K_{CO} K_{H_2} P_{CO} P_{H_2}}{\left(1 + K_{CO}P_{CO} + \sqrt{K_{H_2}P_{H_2}}\right)^2}$$